

---

# LightStereo: Channel Boost Is All Your Need for Efficient 2D Cost Aggregation

---

Xianda Guo<sup>1,\*</sup>, Chenming Zhang<sup>2,3,\*</sup>, Dujun Nie<sup>4,5</sup>, Wenzhao Zheng<sup>6</sup>,  
Youmin Zhang<sup>7,8</sup>, Long Chen<sup>2,3,4,†</sup>

<sup>1</sup> School of Computer Science, Wuhan University

<sup>2</sup> Institute of Artificial Intelligence and Robotics, Xi'an Jiaotong University

<sup>3</sup> Waytous <sup>4</sup> Institute of Automation, Chinese Academy of Sciences <sup>5</sup> Metoak

<sup>6</sup> University of California, Berkeley <sup>7</sup> University of Bologna <sup>8</sup> Rock Universe

## Abstract

We present LightStereo, a cutting-edge stereo-matching network crafted to accelerate the matching process. Departing from conventional methodologies that rely on aggregating computationally intensive 4D costs, LightStereo adopts the 3D cost volume as a lightweight alternative. While similar approaches have been explored previously, our breakthrough lies in enhancing performance through a dedicated focus on the channel dimension of the 3D cost volume, where the distribution of matching costs is encapsulated. Our exhaustive exploration has yielded plenty of strategies to amplify the capacity of the pivotal dimension, ensuring both precision and efficiency. We compare the proposed LightStereo with existing state-of-the-art methods across various benchmarks, which demonstrate its superior performance in speed, accuracy, and resource utilization. LightStereo achieves a competitive EPE metric in the SceneFlow datasets while demanding a minimum of only 22 GFLOPs, with an inference time of just 17 ms. Our comprehensive analysis reveals the effect of 2D cost aggregation for stereo matching, paving the way for real-world applications of efficient stereo systems. Code will be available at <https://github.com/XiandaGuo/OpenStereo>.

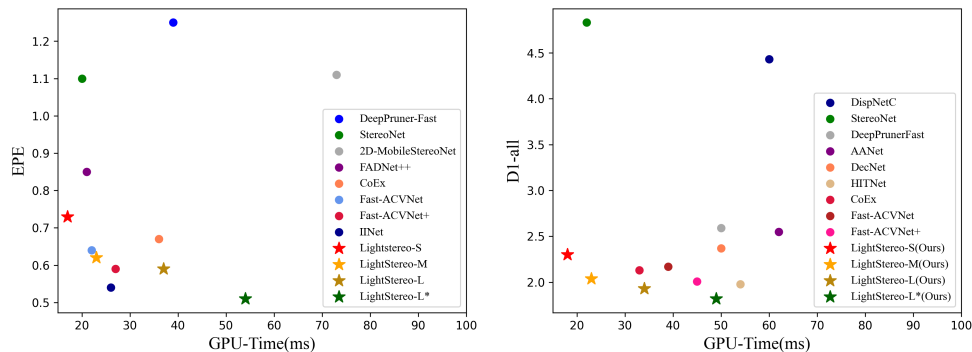


Figure 1: Performance vs. Time on SceneFlow(Left) and KITTI15(Right) datasets.

\*These authors contributed to the work equally.

†Corresponding authors:long.chen@ia.ac.cn

# 1 Introduction

Stereo matching is a pivotal task in computer vision, which aims to ascertain correspondences between points in stereo image pairs to compute depth information. This process underpins numerous applications, including autonomous driving, robotic navigation, and augmented reality. Despite substantial advancements, achieving real-time stereo matching without sacrificing accuracy or efficiency remains a formidable challenge, especially on resource-constrained platforms.

Recent developments [20, 4, 13, 62, 63, 10, 6, 46, 40, 23, 26, 53, 33, 12] have primarily focused on leveraging deep learning techniques for accurate stereo matching. Most methods are based on 3D CNN for cost aggregation. The pioneer is GCNet [20] which jointly learns geometry and context by employing 3D CNN for cost aggregation. Due to the disparity dimension being restored in the constructed 4D cost volume, the network can perform exhaustively aggregation for accurate matching. Following works [4, 13] also adopt this diagram and make notable advancements in performance. To mitigate the expenses in memory and computation of 3D cost aggregation, GANet [62] proposes semi-global guided aggregation and local guided aggregation modules to replace 3D CNNs. LEAStereo [6] utilizes a neural architecture search approach to automatically discover efficient and effective 3D cost aggregation architectures in stereo matching. CoEx [1] employs a guided cost volume excitation approach to facilitate real-time stereo matching with enhanced accuracy. However, the use of 3D CNNs for cost aggregation in CoEx presents challenges for deployment on edge devices due to their computational demands. Another line of work is leveraging iterative refinement at multiple levels [25, 54, 12, 49] to refine disparity prediction on constructed all-pair 3D cost volume. Nevertheless, the overall runtime of these iterative-based methods is over 100ms on a custom GPU.

There are also efforts [47, 48, 38, 57, 56] focusing on lightweight design for stereo matching. AANet [57] constructs a 3D cost volume by correlating the left and right images and introduces intra-scale and cross-scale 2D cost aggregation modules to enhance the efficiency and accuracy of cost aggregation. MobilenetStereo-2D [38] introduces MobileNet [32, 36] blocks to reduce the cost, but the performance is far from satisfaction (EPE 1.14). Overall, these methods based on 2D cost aggregation perform poorly. Cost aggregation is critical to accuracy and efficiency in stereo matching yet existing methods require a compromise between accuracy and speed. However, existing methodologies often necessitate a trade-off between accuracy and processing speed. This paper poses the question: Is it possible to design a lightweight 2D encoder-decoder aggregation net to achieve precise disparity estimation?

From the perspective of cost aggregation in stereo matching, focusing on the disparity channel dimension presents several advantages. Firstly, it allows for more direct modeling of the disparities between corresponding image points, which is crucial for accurate disparity estimation. By focusing on this dimension, it becomes possible to more effectively capture and assimilate the critical information needed for robust stereo matching. In this paper, we propose LightStereo as a positive solution. We explore 2D cost aggregation for stereo matching and leverage inverted residual blocks to enhance both accuracy and computational efficiency. The model is specifically designed to address the challenges of real-time stereo vision applications, focusing on reducing computational demands without compromising the quality of disparity estimation. Specifically, we utilize inverted residual blocks for 2D cost aggregation in stereo matching, which focuses on the disparity channel dimension of the 3D cost volume rather than the dimension of height and width. In inverted residual blocks, the expansion phase increases the channel dimension, allowing the network to learn richer features at a reduced computational cost before compressing them back. In addition, inspired by the effectiveness of large kernel and strip convolutions in image segmentation [35, 17, 11], we propose a Multi-Scale Convolutional Attention Module (MSCA) module for enhancing cost aggregation by extracting features from the left image. By leveraging multi-scale image features to excite the channel dimension of the cost volume, we utilize semantic information inherent in the images (such as object-level semantic details) to guide the cost aggregation process. When encountering discontinuities in disparity, the network halts propagation.

Our main contributions are as follows:

- We propose LightStereo, which achieves a competitive epe in the SceneFLow [30] datasets while demanding a minimum of only 22 Gflops with an inference time of 17 ms.
- We propose inverted residual blocks for 2D cost aggregation in stereo matching.

- We propose the MSCA module for enhancing cost aggregation by extracting features from the left image.
- We verify the effectiveness of LightStereo, achieving SOTA performance on the Scene-flow [30] and KITTI [9, 31] benchmark within the lightweight stereo-matching methods.

## 2 Related Work

Stereo matching, which predicts disparities (depth) from stereo images, can be classified into Conventional and deep-learning-based methods. Regardless of the method studied over the past few decades, researchers have constantly searched for the best trade-off between accuracy and speed to achieve better performance.

### 2.1 Conventional Stereo Matching

Stereo algorithms usually include the following four steps [37]: matching cost computation, cost aggregation, disparity computation/optimization, and disparity refinement. For correspondence problems in cost aggregation, the local method only uses the gray level, color, gradient, and other information of a certain neighborhood to calculate the matching cost, which has low computational complexity [15, 2, 16]. Instead, Global approaches use pixel-based matching cost to search for disparity assignments that minimize the energy function over the entire stereo pair [44] and relative research mainly focuses on minimization procedure being used such as Graph Cut [3], Markov Random Fields [59] and Dynamic Programming [34]. Combined with the above two methods, SGM [14] still adopts the global framework, but uses a more efficient one-dimensional path aggregation method to replace the two-dimensional minimization algorithm. SGM [14] significantly improves the algorithm’s efficiency while being competitive with global algorithms in terms of accuracy.

### 2.2 Deep-learning-based Stereo Matching

To deal with the problem of specular surfaces, ambiguous regions, repetitive patterns, occlusions, and discontinuities, many modern studies use deep learning approaches to replace some or even all steps in the traditional matching process. These deep-learning-based stereo-matching algorithms can be categorized into two groups: accuracy-enhanced and real-time optimized.

**Accuracy-Focused Stereo Matching.** Many contemporary stereo-matching methods are dedicated to enhancing accuracy through various techniques and optimizations. Among these, 3D end-to-end networks have introduced significantly heightened precision in disparity estimation within stereo matching [4, 13, 6, 53, 54, 12]. PSMNet [4] adopts an architecture that leverages spatial pyramid pooling and 3D convolutional neural networks to learn disparity estimation from stereo images. GwcNet [13] introduces a novel approach for constructing the cost volume in stereo matching using group-wise correlation. By dividing left and right features into groups along the channel dimension, correlation maps are computed within each group to generate multiple matching cost proposals. LEAStereo [6] employs a hierarchical neural architecture search (NAS) framework to enhance deep stereo matching performance. IGEV [54] constructs a unified geometry encoding volume, integrating geometry, contextual cues, and local matching intricacies. OpenStereo [12] conducted a comprehensive benchmark with a focus on practical applicability and introduced StereoBase, which further elevates the performance ceiling of stereo matching. To further optimize Stereo matching methods based on iterative optimization, Selective-IGEV [49] proposes the Selective Recurrent Unit to help integrate disparity information across frequencies, minimizing loss during iterative steps. In addition, work [58] improves the loss function by introducing ADL, an adaptive multi-modal cross-entropy loss, to guide network learning of diverse pixel distribution patterns.

**Real-Time-Focused Stereo Matching.** To facilitate the real-time deployment of stereo-matching algorithms, a multitude of strategies have been proposed to optimize their practical application. StereoNet [21] uses color inputs to guide hierarchical refinement and can recover high-frequency details. DeepPruner[8] proposes a PatchMatch module with learnable parameters to save memory and computation by gradually trimming the disparity space to be searched for each pixel. AnyNet[50] has a 2D image convolutional network and a 3D cost tensor convolutional network. It computes disparity estimates at any time by continuously refining the disparity map resolution using the up-sampling method. FADNet[47] leverages efficient 2D correlation layers with residual structures

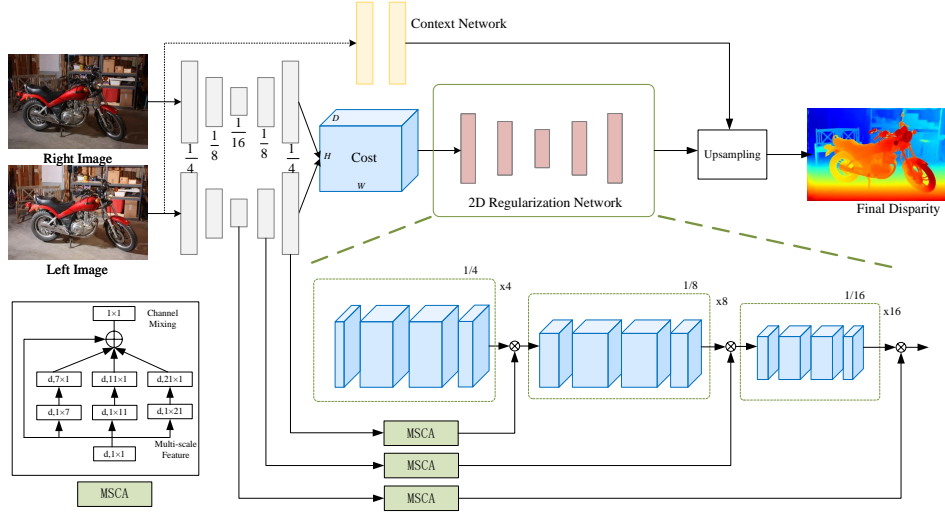


Figure 2: The diagram above illustrates the architecture of LightStereo. MSCA refers to Multi-Scale Convolutional Attention module.

to perform multi-scale predictions. Based on the learned bilateral grid, BGNet[52] designs an edge-preserving cost volume up-sampling module, allowing computationally expensive operations such as 3D convolution to be performed at low resolution. CoEx[1] uses image feature-guided weights and cost volume to excite 3D CNN to extract relevant geometric features. Building upon the foundation of StereoNet [21], MobileStereoNet[38] introduces two stereo vision models suitable for resource-constrained devices, achieving substantial reductions in both parameters and computational operations. However, existing stereo-matching methods still have considerable room for improvement in terms of computational efficiency and parameter scale.

After carefully considering and testing various network structures, we propose a lightweight network, called LightStereo. This model innovatively explores 2D cost aggregation for stereo matching, leveraging advanced techniques to enhance both accuracy and computational efficiency.

### 3 Method

In the deployment of stereo matching on edge devices, constructing a 4D cost volume and using 3D CNNs for cost aggregation prove to be extremely inefficient. Our objective is to construct a 3D cost volume and utilize 2D CNNs, augmented with channel boost, for cost aggregation. This approach aims to maintain a balance between efficiency and accuracy, making it more suitable for real-time applications on resource-constrained devices. Our proposed LightStereo, as depicted in Figure 2, utilizes inverted residual blocks to aggregate disparity from a low-resolution cost volume. In this section, we first describe the design of channel-boosted inverted residual blocks for 2D cost aggregation (Section 3.1). Then, we introduce the Multi-Scale Convolutional Attention (MSCA) (Section 3.2). Finally, in Section 3.3, we present details of the network architecture of LightStereo.

#### 3.1 Inverted Residual Blocks for 2D Cost Aggregation

Previous efforts, such as MobilenetStereo-2D [38], have incorporated MobileNet [32, 36] blocks to decrease computational costs. Despite these efforts, the results have not met expectations, with an EPE of 1.14 on SceneFlow [30] still being reported. To address this issue, our study introduces inverted residual block to boost disparity estimation accuracy. As shown in Figure 3 (c), the inverted residual block [36] is a fundamental component in the design of a lightweight stereo matching network. Given the cost volume whose size is  $H/4 \times W/4 \times Disp/4$ , the key idea is first to boost the number of disparity channels, then apply depthwise convolution, and finally project the expanded features back to a lower-dimensional space, enhancing feature representation significantly. As shown

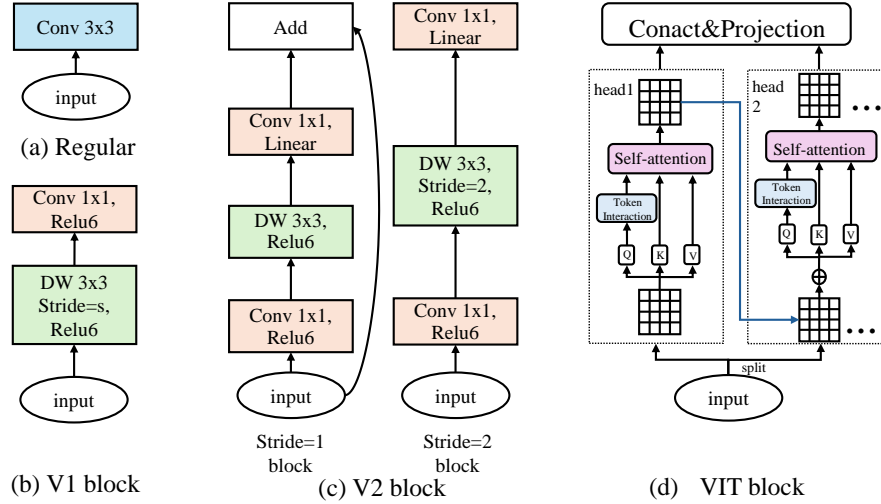


Figure 3: Comparison of different blocks for cost aggregation. DW refers to depthwise separable convolution. V1 Block represents the depthwise separable convolution [32]. V2 Block represents an inverted residual block [36]. ViT Block refers to the block used in EfficientViT [28].

in Figure 2, inverted residual blocks are utilized at resolutions of  $1/4$ ,  $1/8$ , and  $1/16$ , with each resolution corresponding to different blocks. For every block:

Initially, the cost volume  $\mathbf{C}$  is first passed through a  $1 \times 1$  convolution to increase the number of disparity channel:

$$\mathbf{y} = \sigma(\mathbf{W}_{\text{expand}} * \mathbf{C}), \quad (1)$$

where  $\mathbf{W}_{\text{expand}}$  represents the weights of the expansion convolution,  $*$  denotes the convolution operation, and  $\sigma$  is the ReLU6 activation function. Next, the expanded feature map  $\mathbf{y}$  undergoes a  $3 \times 3$  depthwise convolution, which operates independently on each disparity channel to capture spatial features:

$$\mathbf{z} = \sigma(\mathbf{W}_{\text{depthwise}} * \mathbf{y}), \quad (2)$$

where  $\mathbf{W}_{\text{depthwise}}$  are the weights of the depthwise convolution. Finally, the result  $\mathbf{z}$  is then passed through another  $1 \times 1$  convolution to reduce the number of channels back to the original dimension:

$$\mathbf{out} = \mathbf{W}_{\text{project}} * \mathbf{z}, \quad (3)$$

where  $\mathbf{W}_{\text{project}}$  represents the weights of the projection convolution. If the input and output dimensions match, a skip connection is added to improve gradient flow and model performance:

$$\mathbf{out} = \mathbf{out} + \mathbf{x} \quad \text{if dimensions match.} \quad (4)$$

The inverted residual block’s structure significantly reduces computational complexity, making it ideal for resource-constrained environments. Our experimental results demonstrate the superiority of the inverted residual block design compared to regular CNN block (Figure 3 (a)), V1 block [32] (Figure 3 (b)), and Vision Transformer (ViT) block [28] (Figure 3 (d)).

### 3.2 Multi-Scale Convolutional Attention Module

Inspired by the effectiveness of large kernel and strip convolutions in image segmentation [35, 17, 11], we propose a Multi-Scale Convolutional Attention Module (MSCA) module for enhancing cost aggregation by extracting features from the left image. The bottom-left corner of Figure 2 illustrates the architecture of the Multi-Scale Convolutional Attention (MSCA) module. This module is designed to capture and integrate features at multiple scales to enhance the feature representation for cost aggregation. The MSCA incorporates a series of depthwise separable convolutions with varying kernel sizes, specifically  $1 \times 1$ ,  $7 \times 1$ ,  $1 \times 7$ ,  $11 \times 1$ ,  $1 \times 11$ ,  $21 \times 1$ , and  $1 \times 21$ . These convolutions capture both horizontal and vertical strip-like features, which are crucial for identifying elongated

structures within the image. The reason we choose depth-wise strip convolutions is that they are lightweight. For example, by using a pair of  $7 \times 1$  and  $1 \times 7$  convolutions, we can effectively replace a standard  $7 \times 7$  convolution. Thus, strip convolutions serve as a complement to grid convolutions and aid in extracting strip-like features of left images. Utilizing multi-scale image features, MSCA enhances the channel dimension of the cost volume. MSCA incorporates semantic information embedded within the images to direct the cost aggregation process. The network is designed to cease propagation upon detecting disparities that are discontinuous.

Given a stereo image input of size  $H \times W \times 3$ , the method obtains three scales of feature maps at  $1/4$ ,  $1/8$ , and  $1/16$  of the original resolution, respectively. Then, these multi-scale feature maps are then processed by the MSCA module to further extract horizontal and vertical strip-like features. The outputs of MSCA are then concatenated to form a comprehensive multi-scale feature representation. This aggregated feature is subsequently processed by a  $1 \times 1$  convolution, which acts as a channel mixer. The  $1 \times 1$  convolution blends the multi-scale features and recalibrates the feature channels, enhancing the network’s ability to focus on relevant information across different scales. After the MSCA processing, the final output is combined with the aggregated cost by multiplication, enhancing the precision of cost aggregation.

### 3.3 Network Architecture of LightStereo

Our proposed LightStereo consists of five components: feature extraction, cost computation, cost aggregation, disparity prediction, and loss. In the following, we provide introductions to each module.

**Multi-scale Feature Extraction.** For a stereo image pair input with dimensions  $H \times W \times 3$ , our methodology harnesses a MobileNetV2 [1, 54] model, previously trained on the ImageNet [7] dataset, serving as the core architectural foundation. We enable the extraction of feature maps across four distinct scales, effectively reducing the resolution to  $1/4$ ,  $1/8$ ,  $1/16$ , and  $1/32$  of the initial size, respectively. Subsequently, upsampling blocks with skip connections are utilized to restore these feature maps to  $1/4$  scale, which is used to construct the cost volume.

**Cost Volume.** Utilizing the left features  $\mathbf{f}_{l,4}$  and right features  $\mathbf{f}_{r,4}$  extracted from images  $\mathbf{I}_l$  and  $\mathbf{I}_r$ , we construct a correlation volume. The correlation cost volume construction involves comparing features from  $\mathbf{f}_{l,4}$  and  $\mathbf{f}_{r,4}$  across different disparity levels. For each disparity  $d$  within the range of 0 to  $D - 1$ , the similarity between  $\mathbf{f}_{l,4}$  and  $\mathbf{f}_{r,4}$  shifted by  $d$  pixels is computed. Mathematically, this can be expressed as:

$$C_{cor}(d, h, w) = \frac{1}{C} \sum_{c=1}^C f_{l,4}(h, w) \cdot f_{r,4}(h, w - d). \quad (5)$$

For  $d = 0$ , the cost is computed as the average of the element-wise product of feature vectors from  $\mathbf{f}_{l,4}$  and  $\mathbf{f}_{r,4}$  at the same spatial location, across all channels.

**Cost Aggregation.** We use inverted residual blocks to aggregate the cost volume at  $1/4$ ,  $1/8$ , and  $1/16$  resolutions, and at each resolution, we apply multi-scale convolutional attention using the left image, as described in Section 3.1 and Section 3.2. We develop three variants of LightStereo based on block and expansion variations: LightStereo-S for small-scale applications, LightStereo-M for medium-scale tasks, and LightStereo-L. In LightStereo-S, the inverted residual blocks are configured as (1, 2, 4) with an expansion factor of 4. For LightStereo-M, the blocks are set as (4, 8, 14) with an expansion factor of 4. Finally, LightStereo-L utilizes blocks (8, 16, 32) with an expansion factor of 8. LightStereo-L\* denotes that the backbone of LightStereo-L has been replaced with EfficientnetV2 [42].

**Disparity Regression.** We utilize disparity regression [20, 4] to estimate the disparity map. This method predicts disparities by leveraging the probability distribution of each disparity  $d$ , derived from the predicted cost  $c_d$  through the softmax operation  $\sigma(\cdot)$ . The predicted disparity  $\hat{d}$  is then determined by summing each disparity  $d$  weighted by its probability, as depicted by the equation:

$$\hat{d} = \sum_{d=0}^{D_{\max}} d \times \sigma(c_d). \quad (6)$$

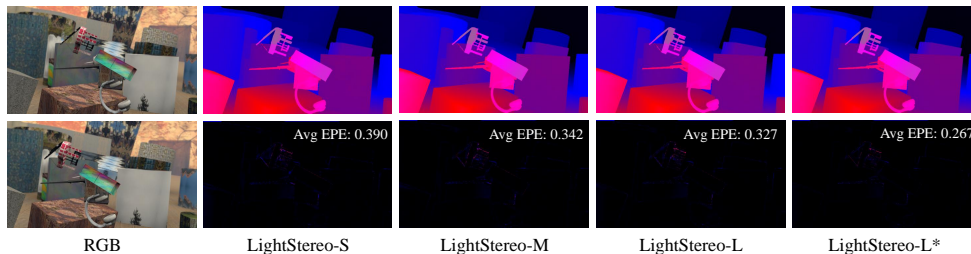


Figure 4: Qualitative results on the test set of SceneFlow [30]. The first column presents the left image on the first row and the right image on the second row. Columns 2 to 5 display the predicted disparity maps on the first row and the corresponding error maps on the second row.

**Loss** We employ the smooth  $L_1$  loss to train the proposed LightStereo. The loss is defined as:

$$L(d, \hat{d}) = \frac{1}{N} \sum_{i=1}^N \text{smooth}_{L_1}(d_i - \hat{d}_i), \quad (7)$$

where  $N$  is the number of labeled pixels,  $d$  represents the ground-truth disparity, and  $\hat{d}$  denotes the predicted disparity.

## 4 Experiment

### 4.1 Datasets and Evaluation Metrics

**SceneFlow**[30] is a synthetic stereo collection that provides 35,454 and 4,370 image pairs for training and testing, respectively. The dataset has a resolution of 960×540 and uses dense disparity maps as ground truth. The data is split into two categories: cleanpass and finalpass. Cleanpass refers to the synthetic images that are generated by clean renderings without post-processing, while finalpass images are produced with photorealistic settings such as motion blur, defocus blur, and noise. In evaluations, we utilize the widely-used metrics the end point error (EPE) as the evaluation metrics.

**KITTI.** KITTI 2012[9] and KITTI 2015[31] are datasets that captured from real-world scenes. KITTI 2012 contains 194 and 195 image pairs for training and testing, respectively. KITTI 2015 provides two sets with 200 image pairs for training and testing. All KITTI datasets provide sparse ground-truth disparities guided by the LiDAR system. For evaluations, we calculate EPE and the percentage of pixels with EPE larger than 3 pixels in all (D1-all) regions. All two KITTI datasets are also used for cross-domain generalization performance evaluation, with EPE and a >3px metric (i.e., the percentage of points with absolute error larger than 3 pixels) reported.

### 4.2 Implementation Details

We have implemented our methods using PyTorch and conducted experiments on 8 NVIDIA RTX 3090 GPUs. For the SceneFlow [30] datasets, the batch sizes for LightStereo-S, LightStereo-M, LightStereo-L, and LightStereo-L\* are set at 24, 12, 8, and 6, respectively. We utilize the AdamW optimizer coupled with OneCycleLR scheduling, where the maximum learning rate was set to 0.0001 multiplied by the batch size. In the ablation study, these LightStereo models were trained over 50 epochs. For the final model evaluation, LightStereo underwent training for 90 epochs. The random crop was used for data augmentation. For the KITTI dataset, we fine-tuned the pre-trained models on the SceneFlow dataset [30] for 500 epochs using a mixed training set comprising KITTI 2012 [9] and KITTI2015 [31] training datasets. We employed a batch size of 2 and utilized the AdamW optimizer. OneCycleLR scheduling was used with a max learning rate of 0.0002. Data augmentation techniques including color jitter, random erase, random scale, and random crop were employed.

Table 1: Comparison with the state-of-the-art on SceneFlow[30]. The runtime is tested on our RTX 3090 GPU.

Method	FLOPs(G)	Params(M)	EPE (px)	Runtime (ms)
DeepPruner-Fast[8]	219.12	7.47	1.25	39
StereoNet[22]	85.93	<b>0.40</b>	1.10	<u>20</u>
2D-MobileStereoNet[38]	128.84	<u>2.23</u>	1.11	73
FADNet++[48]	148.21	124.26	0.85	21
CoEx[1]	53.39	2.72	0.67	36
Fast-ACVNet [55]	79.34	3.08	0.64	22
Fast-ACVNet+ [55]	93.08	3.20	0.59	27
AANet[57]	152.86	2.97	0.87	93
IINet[24]	90.16	19.54	<u>0.54</u>	26
<b>LightStereo-S(Ours)</b>	<b>22.71</b>	3.44	0.73	<b>17</b>
<b>LightStereo-M(Ours)</b>	<u>36.36</u>	7.64	0.62	23
<b>LightStereo-L(Ours)</b>	<u>91.85</u>	24.29	0.59	37
<b>LightStereo-L*(Ours)</b>	159.26	45.63	<b>0.51</b>	54

Table 2: Comparison with the state-of-the-art methods on KITTI benchmarks. The methods are categorized based on whether its runtime exceeds 100ms. Numbers in bold represent the highest values, while numbers underlined indicate the second-highest values. The runtime of the model with \* is tested on our RTX 3090 GPU.

Target	Method	KITTI 2012[9]						KITTI 2015[31]			Runtime (ms)
		3-noc	3-all	4-noc	4-all	EPE noc	EPE all	D1-bg	D1-fg	D1-all	
Accuracy	GANet[62]	1.19	1.60	0.91	1.23	0.4	0.5	1.48	3.46	1.81	1800
	LaC+GANet[27]	1.05	1.42	0.80	1.09	0.4	0.5	1.44	2.83	1.67	1800
	CFNet[39]	1.23	1.58	0.92	1.18	0.4	0.5	1.54	3.56	1.88	180
	SegStereo[60]	1.68	2.03	1.25	1.52	0.5	0.6	1.88	4.07	2.25	600
	SSPCVNet [51]	1.47	1.90	1.08	1.41	0.5	0.6	1.75	3.89	2.11	900
	EdgeStereo-V2[41]	1.46	1.83	1.07	1.34	0.4	0.5	1.84	3.30	2.08	320
	CSPN[5]	1.19	1.53	0.93	1.19	-	-	1.51	2.88	1.74	1000
	LEAStereo[6]	1.13	1.45	0.83	1.08	0.5	0.5	1.40	2.91	1.65	300
	CREStereo[23]	1.14	1.46	0.90	1.14	0.4	0.5	1.45	2.86	1.69	410
	ACVNet [53]	1.13	1.47	0.86	1.12	0.4	0.5	1.37	3.07	1.65	200
Speed	DispNetC[30]	4.11	4.65	2.77	3.20	0.9	1.0	4.32	4.41	4.34	60
	StereoNet [22]	-	-	-	-	0.8	0.9	4.30	7.45	4.83	<u>22</u> *
	DeepPrunerFast[8]	-	-	-	-	-	-	2.32	3.91	2.59	50
	AANet[57]	1.91	2.42	1.46	1.87	0.5	0.6	1.99	5.39	2.55	62
	DecNet[61]	-	-	-	-	-	-	2.07	3.87	2.37	50
	HITNet[43]	<u>1.41</u>	1.89	1.14	1.53	0.4	0.5	1.74	3.20	1.98	54
	CoEx[1]	1.55	1.93	1.15	1.42	0.5	0.5	1.79	3.82	2.13	33
	Fast-ACVNet[55]	1.68	2.13	1.23	1.56	0.5	0.6	1.82	3.93	2.17	39
	Fast-ACVNet+[55]	1.45	<u>1.85</u>	<u>1.06</u>	1.36	0.5	0.5	<u>1.70</u>	3.53	2.01	45
	<b>LightStereo-S (Ours)</b>	1.88	2.34	1.30	1.65	0.6	0.6	2.00	3.80	2.30	<b>17*</b>
	<b>LightStereo-M (Ours)</b>	1.56	1.91	1.10	1.36	0.5	0.5	1.81	3.22	2.04	23*
	<b>LightStereo-L (Ours)</b>	1.55	1.87	1.10	<u>1.33</u>	0.5	0.5	1.78	<b>2.64</b>	1.93	34*
<b>LightStereo-L*(Ours)</b>	<b>1.34</b>	<b>1.62</b>	<b>0.96</b>	<b>1.17</b>	0.5	0.5	<b>1.60</b>	<u>2.92</u>	<b>1.82</b>	49*	

### 4.3 Comparisons with State-of-the-art Methods

As shown in Table 1, we compare our proposed LightStereo methods with several state-of-the-art stereo matching approaches on the SceneFlow [30] dataset. In terms of runtime, LightStereo-S achieves a runtime of only 17ms. This is substantially lower than other methods. Regarding model complexity, LightStereo-S strikes a favorable balance with only 22.71Gflops, comparable to StereoNet [22] (85.93Gflops). This reflects our commitment to maintaining a lightweight model while ensuring competitive performance. In terms of accuracy, LightStereo-L\* achieves an EPE of 0.51, which although slightly higher than some methods like Fast-ACVNet+ [55] (0.59) and IINet [24](0.54), remains competitive while offering significantly lower computational costs. Overall, our LightStereo framework, particularly the LightStereo-S configuration, presents a compelling solution for real-time stereo matching, offering a favorable trade-off between computational efficiency and depth estimation accuracy. This makes it highly suitable for applications such as autonomous navigation and augmented reality, where rapid and reliable depth perception is essential. Figure 4 presents the visualization results of the four proposed models on the SceneFlow [30] dataset. Additionally, we



Table 3: Ablation study of backbone on SceneFlow [30].

Backbone	Type	EPE (px)	Flops(G)	Param(M)	time(ms)
MobilenetV2 [36]	CNN	0.7144	35.82	7.54	22.93
MobilenetV3 [18]	CNN	0.7292	35.72	9.16	25.02
StarNet [29]	CNN	0.7247	40.21	8.98	26.63
EfficientnetV2 [42]	CNN	0.6130	103.14	28.87	46.83
RepViT [45]	Transformer	0.6823	50.45	9.56	28.65

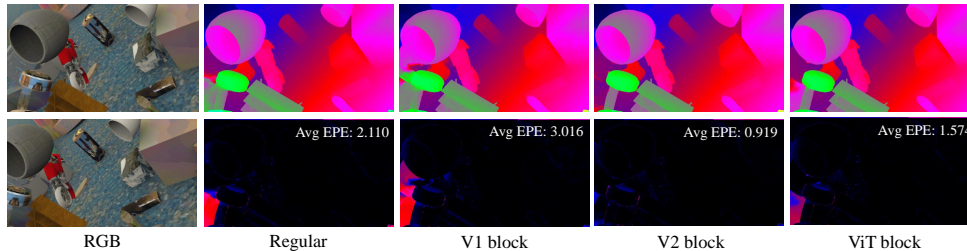


Figure 5: Qualitative results on the test set of SceneFlow [30]. The first column presents the left image on the first row and the right image on the second row. Columns 2 to 5 display the predicted disparity maps on the first row and the corresponding error maps on the second row.

evaluated the results of our proposed models on the KITTI 2012 and 2015 benchmarks. As illustrated in Table 2, the runtime of LightStereo-S exceeds all methods. Notably, LightStereo-L\* surpasses all other lightweight state-of-the-art stereo matching networks across every evaluation metric on the KITTI12 dataset. Additionally, LightStereo-L\* achieved top performance on the KITTI15 dataset in terms of D1-bg and D1-all metrics among lightweight stereo matching methods.

#### 4.4 Ablation Study

**Backbone.** This paper aims to design a lightweight stereo-matching model. To achieve this, we explored the use of classic lightweight models as backbones. As illustrated in Table 3, MobilenetV2 [36] demonstrated a balanced performance with an EPE of 0.7144, FLOPs of 35.82G, 7.54M parameters, and an inference time of 22.93ms. Although MobilenetV3 [18] had slightly lower FLOPs at 35.72G, it showed a higher EPE of 0.7292 and required more parameters (9.16M) with a longer inference time (25.02ms). StarNet [29] exhibited an EPE of 0.7247 with higher FLOPs (40.21G) and inference time (26.63ms). EfficientnetV2 [42] achieved the lowest EPE of 0.6130, but at the cost of significantly higher computational resources (103.14G FLOPs) and parameters (28.87M), with an inference time of 46.83ms. RepViT [45], a transformer-based model, showed an EPE of 0.6876 but required 50.45GFLOPs and 9.56M parameters with an inference time of 28.65ms. Therefore, MobilenetV2 is chosen for its overall efficiency and balance between accuracy and computational cost.

**Conv. Type.** As illustrated in Table 4, our experiments highlight the critical importance of disparity dimensions in the cost aggregation process of stereo matching, rather than spatial expansions in the height and width dimensions. Regular convolutions with different kernel sizes showed that increasing kernel size resulted in higher EPE and significantly increased computational cost. Specifically, expanding the receptive field in the height and width dimensions did not significantly contribute to performance improvement. This finding indicates that merely increasing the spatial extent of convolutions does not effectively enhance the accuracy of stereo-matching. Instead, the emphasis should be placed on optimizing the disparity dimensions to improve the aggregation of cost volumes, as this approach is more effective in capturing relevant features and enhancing overall performance. The V1 block with a  $3 \times 3$  kernel showed an EPE of 0.7801, indicating moderate performance with reduced FLOPs (34.86G), but it had a higher inference time (54.21ms). In contrast, the V2 block provided the best balance, achieving the lowest EPE of 0.7144, and FLOPs of 35.82G, with an inference time of 22.93ms. This superior performance is attributed to the structure of the V2 block, which incorporates expansion convolutions in the disparity dimension. By focusing on enhancing the disparity dimensions rather than merely expanding the spatial dimensions, the V2 block effectively aggregates cost volumes, leading to improved accuracy and efficiency in stereo-matching tasks. The

Table 4: Ablation study on the design of the block on SceneFLow [30]. Regular represents regular convolution. V1 Block represents the depthwise separable convolution [32]. V2 Block represents an inverted residual block [36]. DW refers to depthwise separable convolution. ViT Block refers to the block used in EfficientViT [28]. The underlined backbone is the one we ultimately used.

Conv. Type	Kernel	Block	EPE (px)	Flops(G)	Param(M)	time(ms)
Regular	$3 \times 3$	(4 8 16)	0.7652	36.27	8.04	22.75
Regular	$5 \times 5$	(4 8 16)	0.7979	71.16	18.62	17.61
Regular	$7 \times 7$	(4 8 16)	0.8190	123.51	34.49	20.06
Regular	$11 \times 11$	(4 8 16)	0.8672	280.53	82.10	34.22
V1 Block	DW $3 \times 3$	(30 60 120)	0.7801	34.86	7.57	54.21
<u>V2 Block</u>	DW $3 \times 3$	(4 8 16)	0.7144	35.82	7.54	22.93
ViT Block	-	(3 6 9)	0.7149	34.48	6.53	51.14

ViT block showed a similar EPE to the V2 block but had a lower parameter count (6.53M) and higher inference time (51.14ms). Ultimately, the V2 block was chosen for its optimal balance between accuracy and computational efficiency. Figure 5 shows a visual comparison with different conv. type. It can be observed that for the occluded area in the lower left corner of the left image, the cost aggregation based on the V2 block achieves better results than the other 3 conv. type.

**Block Structure Analysis.** As illustrated in Table 5, we explore the impact of different block structures while maintaining a constant expansion factor of 4. Configurations 'e' to 'h' explore blocks (1, 2, 4), (2, 4, 8), (4, 8, 16), and (8, 16, 32) respectively. The results show that larger blocks generally lead to better performance. For instance, configuration 'e' with the smallest block (1, 2, 4) has the highest EPE of 0.8317, while configuration 'h' with the largest block (8, 16, 32) shows an improvement in EPE, but detailed metrics are not provided. There is a trade-off between accuracy and computational cost, as larger blocks increase FLOPs and parameters.

**Expansion Factor Analysis.** As illustrated in Table 5, we further analyze the effect of varying expansion factors while keeping the block structure constant. As the expansion factor increases, a consistent decrease in EPE is observed, indicating improved accuracy. Specifically, configuration 'a' with an expansion factor of 2 has an EPE of 0.7557, while configuration 'd' with an expansion factor of 16 achieves the lowest EPE of 0.6650. The analysis further proves that the critical importance of disparity dimensions cannot be overstated in the cost aggregation process of stereo matching. The disparity dimension is pivotal in effectively aggregating cost volumes, leading to more accurate and reliable depth estimations. However, this improvement in accuracy comes at the cost of significantly increased computational complexity and parameters, with flops increasing from 26.23G to 93.34G and the inference time increases from 22.44ms to 36.67ms.

**MSCA Module Analysis.** As illustrated in Table 5, the baseline configuration (i) with blocks (4, 8, 16) achieved an EPE of 0.7144. Incorporating MSCA (configuration k) reduced the EPE further to 0.6809 with minimal changes in FLOPs and parameters. This suggests that MSCA provides the most significant improvement in accuracy with minimal impact on computational efficiency. We also explored the use of the SE module [19]. Configurations 'i' to 'j' show that although the SE module improves accuracy, reducing EPE from 0.7144 to 0.7036. However, this improvement comes with an increase in parameters from 7.54M to 12.76M and a slight increase in FLOPs and inference time.

#### 4.5 Runtime Analysis

As shown in Table 6, it is evident that the LightStereo framework demonstrates commendable efficiency across its constituent modules. Each component, including feature extraction, cost computation, cost aggregation, and disparity regression, contributes to the overall computational time. It is evident that as the number of blocks increases, the time required for cost aggregation in LightStereo-S, LightStereo-M, and LightStereo-L also increases. For LightStereo-L\*, the time spent on feature extraction is extended due to the adoption of a more complex EfficientNetV2. These runtime breakdowns underscore the effectiveness of the LightStereo framework in achieving real-time stereo-matching capabilities.

Table 5: Ablation study on the design of the block on SceneFlow [30]. Expansion refers to the expansion factor. SE represents Squeeze-and-Excitation [19]. MSCA represents Multi-Scale Convolutional Attention.

	Block	Expansion	SE	MSCA	EPE (px)	Flops(G)	Param(M)	time(ms)
a	(4 8 16)	(2 2 2)			0.7557	26.23	4.81	22.44
b	(4 8 16)	(4 4 4)			0.7144	35.82	7.54	22.93
c	(4 8 16)	(8 8 8)			0.6853	54.99	12.99	23.59
d	(4 8 16)	(16 16 16)			0.6650	93.34	23.90	36.67
e	(1 2 4)	(4 4 4)			0.8317	22.17	3.34	16.65
f	(2 4 8)	(4 4 4)			0.7464	26.72	4.74	20.04
g	(4 8 16)	(4 4 4)			0.7144	35.82	7.54	22.93
h	(8 16 32)	(4 4 4)			0.6973	54.02	13.14	31.09
i	(4 8 16)	(4 4 4)			0.7144	35.82	7.54	22.93
j	(4 8 16)	(4 4 4)	✓		0.7036	35.90	12.76	30.14
k	(4 8 16)	(4 4 4)		✓	0.6809	36.36	7.64	23.14
l	(4 8 16)	(4 4 4)	✓	✓	0.6810	36.44	12.86	30.82
m	(1 2 4)	(4 4 4)		✓	0.7899	22.71	3.44	17.59
n	(4 8 16)	(4 4 4)		✓	0.6809	36.36	7.64	23.14
o	(8 16 32)	(8 8 8)		✓	0.6382	91.85	24.29	37.55

Table 6: Runtime breakdown.

Module	Feature Extraction	Cost	Cost Aggregation	Disparity Regression	Total Time
LightStereo-S	10.39	1.98	3.98	1.48	17.83
LightStereo-M	10.39	1.98	9.59	1.49	23.45
LightStereo-L	10.39	1.98	23.64	1.49	37.50
LightStereo-L*	27.17	1.98	23.64	1.49	54.28

## 5 Conclusion

In conclusion, this paper designs a lightweight 2D encoder-decoder aggregation net to achieve precise and fast disparity estimation, called LightStereo. While similar approaches have been explored previously, our novel contribution lies in optimizing performance through a targeted emphasis on the disparity channel dimension within the 3D cost volume, which encapsulates the distribution of matching costs. Our exhaustive exploration has led to the development of numerous strategies to enhance the capacity of this crucial dimension, ensuring both precision and efficiency in disparity estimation. LightStereo offers a compelling solution for accelerating the matching process while maintaining high levels of accuracy and efficiency.

**Acknowledgements.** This work was supported by the National Natural Science Foundation of China under Grant 62373356 and the Open Projects Program of the State Key Laboratory of Multimodal Artificial Intelligence Systems.

## References

- [1] Antyanta Bangunharcana, Jae Won Cho, Seokju Lee, In So Kweon, Kyung-Soo Kim, and Soohyun Kim. Correlate-and-excite: Real-time stereo matching via guided cost volume excitation. In *IROS*, 2021.
- [2] Michael Bleyer, Christoph Rhemann, and Carsten Rother. Patchmatch stereo-stereo matching with slanted support windows. In *Bmvc*, 2011.
- [3] Yuri Boykov, Olga Veksler, and Ramin Zabih. Fast approximate energy minimization via graph cuts. *TPAMI*, 2001.
- [4] Jia-Ren Chang and Yong-Sheng Chen. Pyramid stereo matching network. In *CVPR*, 2018.
- [5] Xinjing Cheng, Peng Wang, and Ruigang Yang. Learning depth with convolutional spatial propagation network. *TPAMI*, 2019.

- [6] Xuelian Cheng, Yiran Zhong, Mehrtash Harandi, Yuchao Dai, Xiaojun Chang, Hongdong Li, Tom Drummond, and Zongyuan Ge. Hierarchical neural architecture search for deep stereo matching. In *NeurIPS*, 2020.
- [7] Jia Deng, Wei Dong, Richard Socher, Li-Jia Li, Kai Li, and Li Fei-Fei. ImageNet: A large-scale hierarchical image database. In *CVPR*, 2009.
- [8] Shivam Duggal, Shenlong Wang, Wei-Chiu Ma, Rui Hu, and Raquel Urtasun. Deeppruner: Learning efficient stereo matching via differentiable patchmatch. In *ICCV*, 2019.
- [9] Andreas Geiger, Philip Lenz, and Raquel Urtasun. Are we ready for autonomous driving? the kitti vision benchmark suite. In *CVPR*, 2012.
- [10] Xiaodong Gu, Zhiwen Fan, Siyu Zhu, Zuozhuo Dai, Feitong Tan, and Ping Tan. Cascade cost volume for high-resolution multi-view stereo and stereo matching. In *CVPR*, 2020.
- [11] Meng-Hao Guo, Cheng-Ze Lu, Qibin Hou, Zhengning Liu, Ming-Ming Cheng, and Shi-Min Hu. Segnext: Rethinking convolutional attention design for semantic segmentation. *NeurIPS*, 2022.
- [12] Xianda Guo, Juntao Lu, Chenming Zhang, Yiqi Wang, Yiqun Duan, Tian Yang, Zheng Zhu, and Long Chen. Openstereo: A comprehensive benchmark for stereo matching and strong baseline. *arXiv preprint arXiv:2312.00343*, 2023.
- [13] Xiaoyang Guo, Kai Yang, Wukui Yang, Xiaogang Wang, and Hongsheng Li. Group-wise correlation stereo network. In *CVPR*, 2019.
- [14] Heiko Hirschmuller. Accurate and efficient stereo processing by semi-global matching and mutual information. In *CVPR*, 2005.
- [15] Asmaa Hosni, Michael Bleyer, Margrit Gelautz, and Christoph Rhemann. Local stereo matching using geodesic support weights. In *ICIP*, 2009.
- [16] Asmaa Hosni, Christoph Rhemann, Michael Bleyer, Carsten Rother, and Margrit Gelautz. Fast cost-volume filtering for visual correspondence and beyond. *TPAMI*, 2012.
- [17] Qibin Hou, Li Zhang, Ming-Ming Cheng, and Jiashi Feng. Strip pooling: Rethinking spatial pooling for scene parsing. In *CVPR*, 2020.
- [18] Andrew Howard, Mark Sandler, Grace Chu, Liang-Chieh Chen, Bo Chen, Mingxing Tan, Weijun Wang, Yukun Zhu, Ruoming Pang, Vijay Vasudevan, et al. Searching for mobilenetv3. In *ICCV*, 2019.
- [19] Jie Hu, Li Shen, and Gang Sun. Squeeze-and-excitation networks. In *CVPR*, 2018.
- [20] Alex Kendall, Hayk Martirosyan, Saumitro Dasgupta, Peter Henry, Ryan Kennedy, Abraham Bachrach, and Adam Bry. End-to-end learning of geometry and context for deep stereo regression. In *ICCV*, 2017.
- [21] Sameh Khamis, Sean Fanello, Christoph Rhemann, Adarsh Kowdle, Julien Valentin, and Shahram Izadi. Stereonet: Guided hierarchical refinement for real-time edge-aware depth prediction. In *ECCV*, 2018.
- [22] Sameh Khamis, Sean Fanello, Christoph Rhemann, Adarsh Kowdle, Julien Valentin, and Shahram Izadi. Stereonet: Guided hierarchical refinement for real-time edge-aware depth prediction. In *ECCV*, 2018.
- [23] Jiankun Li, Peisen Wang, Pengfei Xiong, Tao Cai, Ziwei Yan, Lei Yang, Jianguo Liu, Haoqiang Fan, and Shuaicheng Liu. Practical stereo matching via cascaded recurrent network with adaptive correlation. In *CVPR*, 2022.
- [24] Ximeng Li, Chen Zhang, Wanjuan Su, and Wenbing Tao. Inet: Implicit intra-inter information fusion for real-time stereo matching. In *AAAI*, 2024.
- [25] Lahav Lipson, Zachary Teed, and Jia Deng. Raft-stereo: Multilevel recurrent field transforms for stereo matching. In *3DV*, 2021.
- [26] Biyang Liu, Huimin Yu, and Yangqi Long. Local similarity pattern and cost self-reassembling for deep stereo matching networks. In *AAAI*, 2022.
- [27] Biyang Liu, Huimin Yu, and Yangqi Long. Local similarity pattern and cost self-reassembling for deep stereo matching networks. In *AAAI*, 2022.
- [28] Xinyu Liu, Houwen Peng, Ningxin Zheng, Yuqing Yang, Han Hu, and Yixuan Yuan. Efficientvit: Memory efficient vision transformer with cascaded group attention. In *CVPR*, 2023.
- [29] Xu Ma, Xiyang Dai, Yue Bai, Yizhou Wang, and Yun Fu. Rewrite the stars. *CVPR*, 2024.
- [30] Nikolaus Mayer, Eddy Ilg, Philip Hausser, Philipp Fischer, Daniel Cremers, Alexey Dosovitskiy, and Thomas Brox. A large dataset to train convolutional networks for disparity, optical flow, and scene flow estimation. In *CVPR*, 2016.
- [31] Moritz Menze and Andreas Geiger. Object scene flow for autonomous vehicles. In *CVPR*, 2015.

- [32] Maad M Mijwil, Ruchi Doshi, Kamal Kant Hiran, Omega John Unogwu, and Indu Bala. Mobilenetv1-based deep learning model for accurate brain tumor classification. *Mesopotamian Journal of Computer Science*, 2023.
- [33] Guang-Yu Nie, Ming-Ming Cheng, Yun Liu, Zhengfa Liang, Deng-Ping Fan, Yue Liu, and Yongtian Wang. Multi-level context ultra-aggregation for stereo matching. In *CVPR*, 2019.
- [34] Yuichi Ohta and Takeo Kanade. Stereo by intra-and inter-scanline search using dynamic programming. *TPAMI*, 1985.
- [35] Chao Peng, Xiangyu Zhang, Gang Yu, Guiming Luo, and Jian Sun. Large kernel matters—improve semantic segmentation by global convolutional network. In *CVPR*, 2017.
- [36] Mark Sandler, Andrew Howard, Menglong Zhu, Andrey Zhmoginov, and Liang-Chieh Chen. Mobilenetv2: Inverted residuals and linear bottlenecks. In *CVPR*, 2018.
- [37] Daniel Scharstein and Richard Szeliski. A taxonomy and evaluation of dense two-frame stereo correspondence algorithms. *IJCV*, 2002.
- [38] Faranak Shamsafar, Samuel Woerz, Rafia Rahim, and Andreas Zell. Mobilestereonet: Towards lightweight deep networks for stereo matching. In *WACV*, 2022.
- [39] Zhelun Shen, Yuchao Dai, and Zhibo Rao. Cfnets: Cascade and fused cost volume for robust stereo matching. *arXiv preprint arXiv:2104.04314*, 2021.
- [40] Xiao Song, Guorun Yang, Xinge Zhu, Hui Zhou, Zhe Wang, and Jianping Shi. Adastereo: A simple and efficient approach for adaptive stereo matching. In *CVPR*, 2021.
- [41] Xiao Song, Xu Zhao, Liangji Fang, Hanwen Hu, and Yizhou Yu. Edgestereo: An effective multi-task learning network for stereo matching and edge detection. *IJCV*, 2020.
- [42] Mingxing Tan and Quoc Le. Efficientnetv2: Smaller models and faster training. In *ICML*, 2021.
- [43] Vladimir Tankovich, Christian Hane, Yinda Zhang, Adarsh Kowdle, Sean Fanello, and Sofien Bouaziz. Hitnet: Hierarchical iterative tile refinement network for real-time stereo matching. In *CVPR*, 2021.
- [44] Demetri Terzopoulos. Regularization of inverse visual problems involving discontinuities. *TPAMI*, 1986.
- [45] Ao Wang, Hui Chen, Zijia Lin, Hengjun Pu, and Guiguang Ding. Reprvit: Revisiting mobile cnn from vit perspective. *CVPR*, 2024.
- [46] Hengli Wang, Rui Fan, Peide Cai, and Ming Liu. Pvsstereo: Pyramid voting module for end-to-end self-supervised stereo matching. *ICRA*, 2021.
- [47] Qiang Wang, Shaohuai Shi, Shizhen Zheng, Kaiyong Zhao, and Xiaowen Chu. FADNet: A fast and accurate network for disparity estimation. In *ICRA*, 2020.
- [48] Qiang Wang, Shaohuai Shi, Shizhen Zheng, Kaiyong Zhao, and Xiaowen Chu. Fadnet++: Real-time and accurate disparity estimation with configurable networks. *arXiv preprint arXiv:2110.02582*, 2021.
- [49] Xianqi Wang, Gangwei Xu, Hao Jia, and Xin Yang. Selective-stereo: Adaptive frequency information selection for stereo matching. 2024.
- [50] Yan Wang, Zihang Lai, Gao Huang, Brian H. Wang, Laurens van der Maaten, Mark Campbell, and Kilian Q. Weinberger. Anytime stereo image depth estimation on mobile devices. In *ICRA*, 2019.
- [51] Zhenyao Wu, Xinyi Wu, Xiaoping Zhang, Song Wang, and Lili Ju. Semantic stereo matching with pyramid cost volumes. In *ICCV*, 2019.
- [52] Bin Xu, Yuhua Xu, Xiaoli Yang, Wei Jia, and Yulan Guo. Bilateral grid learning for stereo matching networks. In *CVPR*, 2021.
- [53] Gangwei Xu, Junda Cheng, Peng Guo, and Xin Yang. Attention concatenation volume for accurate and efficient stereo matching. In *CVPR*, 2022.
- [54] Gangwei Xu, Xianqi Wang, Xiaohuan Ding, and Xin Yang. Iterative geometry encoding volume for stereo matching. In *CVPR*, 2023.
- [55] Gangwei Xu, Yun Wang, Junda Cheng, Jinhui Tang, and Xin Yang. Accurate and efficient stereo matching via attention concatenation volume. *TPAMI*, 2023.
- [56] Gangwei Xu, Huan Zhou, and Xin Yang. Cgi-stereo: Accurate and real-time stereo matching via context and geometry interaction. *arXiv preprint arXiv:2301.02789*, 2023.
- [57] Haofei Xu and Juyong Zhang. Aanet: Adaptive aggregation network for efficient stereo matching. In *CVPR*, 2020.
- [58] Peng Xu, Zhiyu Xiang, Chengyu Qiao, Jingyun Fu, and Tianyu Pu. Adaptive multi-modal cross-entropy loss for stereo matching. 2024.
- [59] Koichiro Yamaguchi, David McAllester, and Raquel Urtasun. Efficient joint segmentation, occlusion labeling, stereo and flow estimation. In *ECCV*, 2014.

- [60] Guorun Yang, Hengshuang Zhao, Jianping Shi, Zhidong Deng, and Jiaya Jia. Segstereo: Exploiting semantic information for disparity estimation. In *ECCV*, 2018.
- [61] Chengtang Yao, Yunde Jia, Huijun Di, Pengxiang Li, and Yuwei Wu. A decomposition model for stereo matching. In *CVPR*, 2021.
- [62] Feihu Zhang, Victor Prisacariu, Ruigang Yang, and Philip H.S. Torr. Ga-net: Guided aggregation net for end-to-end stereo matching. In *CVPR*, 2019.
- [63] Feihu Zhang, Xiaojuan Qi, Ruigang Yang, Victor Prisacariu, Benjamin Wah, and Philip Torr. Domain-invariant stereo matching networks. In *ECCV*, 2020.